Temperature Distribution Measurement and Internal Flow Visualization in the Lubrication Film of Non-contacting Mechanical Seals

Yuki Sato[1] · Masayuki Ochiai[2]

Abstract

The surface textures of non-contacting mechanical seals form a few micrometers thick lubrication film that aids in achieving high performance of the seal. Improved texture design can control internal fluid flow, improving the sealing performance and lubrication characteristics. However, film thickness is sensitive to thermal deformation, making seals vulnerable to heat. Excessive temperature increases and deviations in temperature distribution can cause performance degradation or damage to seals. Previous studies have suggested that heat transfer impacting these thermal issues may be influenced by the internal flow, however, experimental studies examining flow fields have not been conducted yet. This study presents the design of experimental equipment, measurement of temperature distributions and observation of flow fields in lubrication films with three different textures—non-textured, Rayleigh step, and spiral groove. Furthermore, the results were compared with those of numerical analysis. Temperature was found to be higher at the downstream end of the flow. In particular, the Rayleigh step seal exhibited a nonuniform temperature distribution that alternated between low and high-temperature areas. This was caused by cooling related to radial grooves that had a pumping effect. In contrast, a uniform temperature distribution was confirmed in the case of the spiral groove seal, which was formed by mixing outer and inner side fluids. The results indicate that the temperature distribution in lubrication films can be controlled via flow field by the surface texture shape or depth to protect against thermal degradation and to achieve high reliability of non-contacting mechanical seals.

✉ Masayuki Ochiai
ochiaim@keyaki.cc.u-tokai.ac.jp

[1] Graduate School of Engineering, Tokai University, 4-1-1 Kitakaname, Hiratsuka, Kanagawa 259-1292, Japan

[2] Department of Mechanical Engineering, Tokai University, 4-1-1 Kitakaname, Hiratsuka, Kanagawa 259-1292, Japan

Graphical Abstract
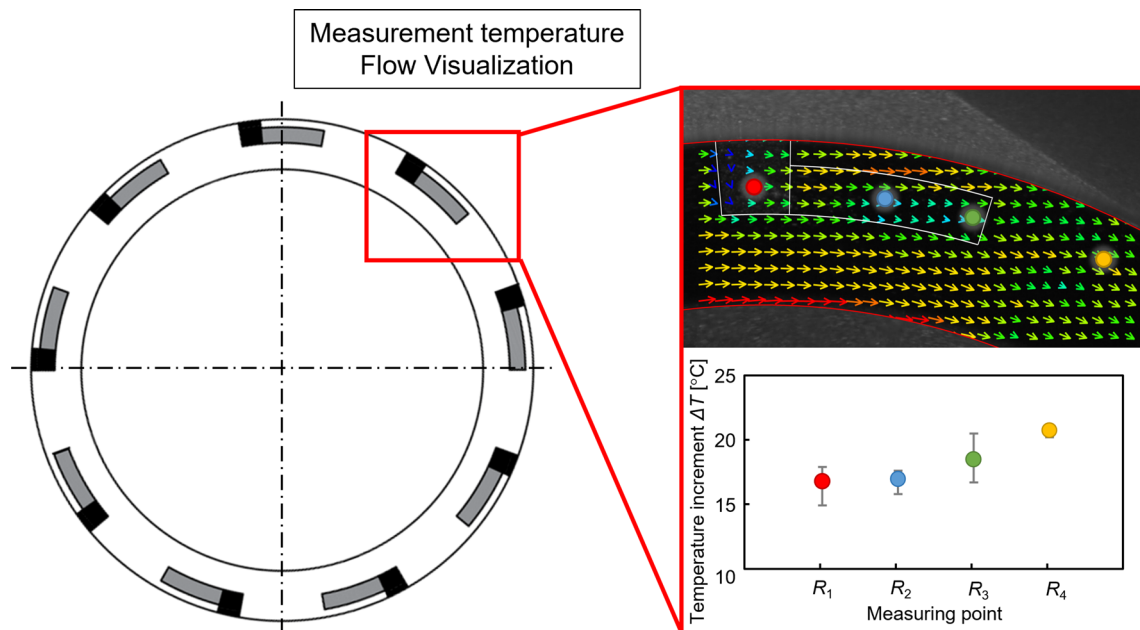
1 Introduction

Non-contacting mechanical seals are used to prevent fluid from leaking around the rotating shaft in turbomachinery. Figure 1 shows the schematic diagram of such seals, which consist of a rotating ring, stationary ring, housing, and springs. Surface textures are processed on the rotating ring to form a lubrication film in the gap between the two rings, which is a few micrometers thick and are sufficiently thin to seal the fluid. Furthermore, because the two rings maintain a non-contacting state, the seals can be used under high-speed and high-pressure conditions. Recently, the operational speed of turbomachinery is increasing, and energy conservation and higher efficiency of these machinery have become necessary. Consequently, the importance of the seals, which are responsible for preventing leakage of hazardous fluid, is increasing, additionally because of the need to reduce the environmental impacts.

The performance of the seals depends considerably on surface textures. Therefore, various shape and depth textures

Fig. 1 Schematic of non-contacting mechanical seals
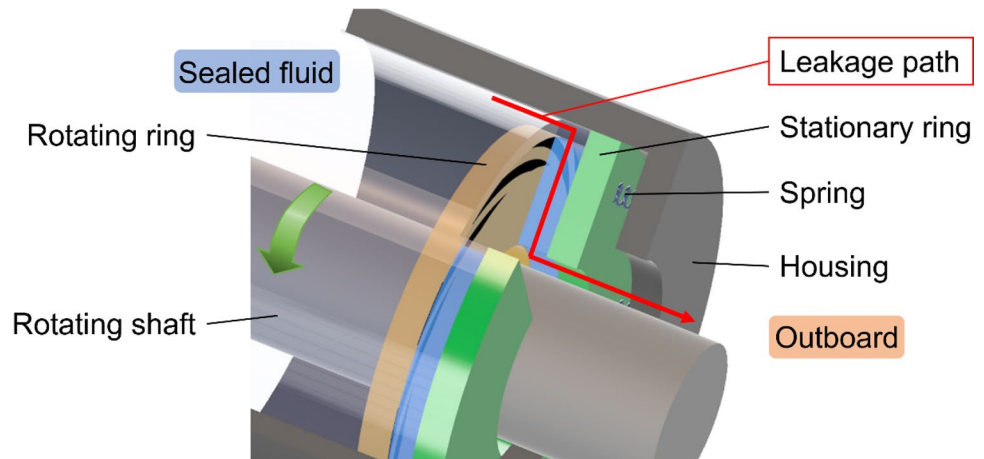
have been proposed [1–6] to achieve better performance by controlling the fluid flow. Ikeuchi et al. [1] presented a groove consisting of a Rayleigh step with a reverse step added to generate negative pressure. The groove improved seal stability by preventing an excessive increase in film thickness under operations at various rotational speeds. Buck et al. [2] also presented spiral grooves that were designed to pump fluid to reduce leakage, enabling a decrease in external fluid pressure. In contrast, Tokunaga et al. [3] attempted to balance the trade-off between sealing and lubrication using an arrangement of Rayleigh steps, used for lubrication, and spiral grooves, used to provide sealing. In recent years, this effect has been shown to promote the formation of the adsorption film of plasma proteins in the blood by surface textures, thereby reducing the friction coefficient [7].

Thus, surface textures have been designed to minimize leakage, improve lubrication characteristics, and address many other challenges. However, the thin lubrication film makes the seals vulnerable to heat, increasing the risk of performance deterioration and damage by thermal deformation and stress [8, 9]. This indicates that, thermal issues degrade the reliability of systems containing the seals by increasing hazardous fluid leaks and making frequent maintenance necessary, which must be considered when designing seals. Several analyses have been conducted examining the impacts of temperature distribution on the properties of films [10–12]. For example, Blasiak et al. [10] analyzed the temperature distribution of rings and fluid with different groove shapes and depths using a numerical solution. They obtained a maximum temperature difference of approximately 30 °C in the circumferential direction and showed that the temperature distributions of the film depended on the surface patterns. They found that the smoother flow of the cold outer fluid increases the difference in temperature distribution affecting the dynamic properties of the film through changes to dynamic viscosity. Teshima [13] experimented with seals containing anisotropic shape dimples, which were based on information provided in previous studies [14, 15] showing that the direction of roughness affects the friction coefficient, load capacity, and temperature increase via changes to the flow field. The study confirmed that the dimples transverse in a sliding direction to suppress the temperature increase and have excellent lubrication characteristics. In this way, previous studies have suggested that internal flow affects the thermal properties of lubrication films, but the flow fields have not been observed yet.

Tokunaga et al. [16] observed cavitation caused by dimples in non-contacting mechanical seals, finding that the cavitation, which was formed by a dimple upstream in the circumferential direction, combined with each other further downstream. Therefore, the circular gas phase area was observed and considered to be valuable for preventing leakage. In addition, Particle Image Velocimetry (PIV) analysis,

a method that calculates velocity vectors by visualizing traceable particles, can be used to evaluate lubricant flow. Cross et al. [17] and Richardson et al. [18] reported flow visualization in pocketed thrust bearings and Ochiai et al. [19] evaluated the squeeze effect in dry gas seals. Strubel et al. [20] observed the meniscus from a ball-on-disk test by using fluorescent particles for PIV analysis and steel particles that imitated contamination. The results showed the flow in the meniscus to be in good agreement with the previous numerical analysis results and that the steel particles that were entrained between the ball and disk deformed to a thickness close to the calculated lubrication film thickness. In this way, visualization, especially PIV analysis, has been used to understand lubrication phenomena.

In this study, we designed an experimental equipment to observe a lubrication film. The effect of internal flow on the temperature distribution of a lubrication film in non-contacting mechanical seals was then considered by measuring the temperature distribution and visualizing the internal flow for each surface texture. Each flow field was evaluated using the results of PIV analysis of captured images. In addition, comparing isothermal numerical solutions with the experimental results, the difference between them was discussed.

2 Experiment

2.1 Test Seals

Rayleigh step, spiral groove, and non-textured seals were tested in this study. Figure 2 shows the texture geometries and Table 1 shows the texture dimensions used in this study. The outer radius of all test seals, r_o, was 32.0 mm and their inner radius, r_i, was 25.6 mm. The Rayleigh step and spiral groove were designed as conventional surface textures based on information provided in previous studies [21–23]. The Rayleigh step was designed to introduce fluid through deep grooves, called radial grooves, and to generate positive pressure and seals at the steps. Spiral grooves were arranged to reduce leakage by pumping atmospheric air from the inner side, by using the flow toward the outer side caused by the hydrodynamic action of grooves as explained in Ref. [2]. The non-textured seal did not have texture.

2.2 Experimental Equipment

Figure 3 shows a schematic of the equipment, which was mounted on an air spring vibration isolator and consisted of a rotor, test seal, chamber, and high-frequency motor. The test seals and chamber were made of acrylic resin for ease of visual observations, and the rotor was made of stainless steel (ISO X10CrNiS 18–9). The rotor was driven directly by the motor below the equipment, and the
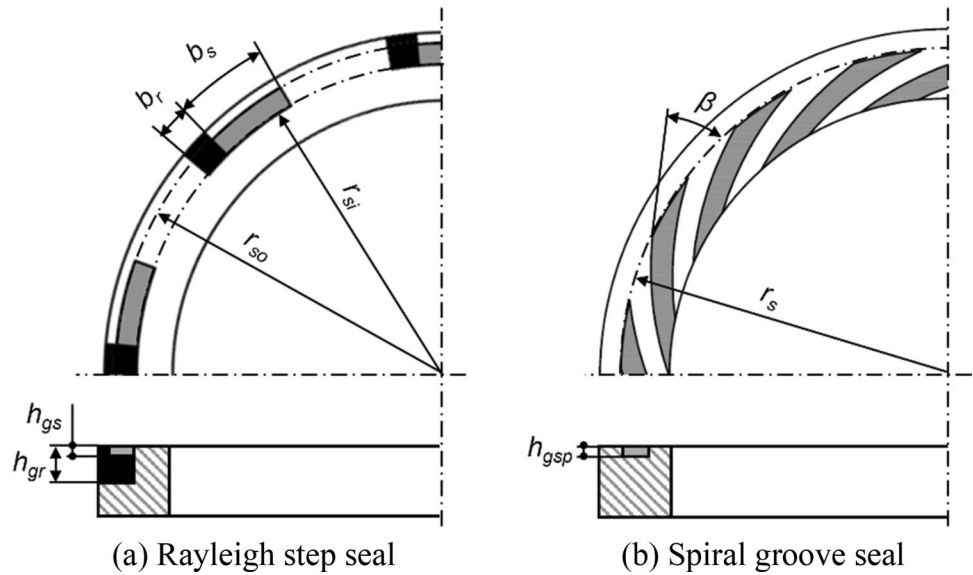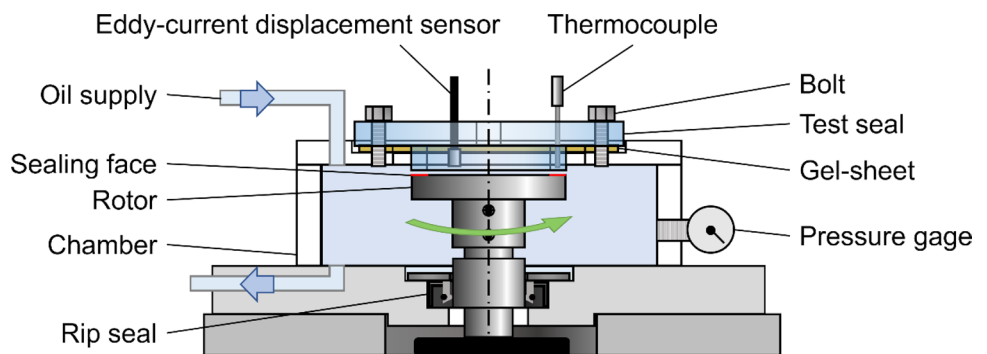
Fig. 2 Texture geometries

(a) Rayleigh step seal   (b) Spiral groove seal

Table 1 Texture dimensions

Rayleigh step seal	
Outer radius of step r_{so}	31.0 mm
Inner radius of step r_{si}	29.0 mm
Number of Rayleigh steps N_{rs}	9
Radial groove width b_r	0.087 rad
Step width b_s	0.26 rad
Radial groove depth h_{gr}	1000 μm
Step depth h_{gs}	50 μm
Spiral groove seal	
Spiral sealing radius r_s	30.0 mm
Spiral angle $β$	0.35 rad
Number of spiral grooves N_{sp}	15
Spiral groove depth h_{gsp}	50 μm

film using the relative motion of the stationary test seal and rotor. The test seal was bolted to the chamber with a gel sheet. The gap between the surface of the test seal and rotor was adjusted by tightening the bolt. The film thickness was measured by three eddy-current displacement sensors (AH-305, KEYENCE) set on the test seal. Since the sensors were mounted against the rotor surface inside the sealing face, thermal expansion during operation was overestimated. Therefore, the sensors were used to set the initial film thickness before operation. Sealed fluid was cooled by a radiator and resupplied to the chamber from a reservoir via pumps. Pressure in the chamber was adjusted by changing the output of the pumps. In this paper, all pressure values are hereafter referred to as gauge pressure. Fluid temperature was measured by sheathed T type thermocouples (TJC36-CPSS-020U-6, OMEGA Engineering) set on the test seal using feedthroughs. The diameter of the sensor tip and accuracy of thermocouples were 0.5 mm and ± 0.5 °C, respectively.

rotational speed was adjusted by changing the output of an inverter. In this way, the equipment replicated lubrication

Fig. 3 Schematic of experimental equipment

2.3 Measurement of Temperature Distribution and Leakage Rate

The seals used to measure the temperature distribution had machined pores of diameter 1.0 mm at each measurement point as shown in Fig. 4. Thermocouples were set such that the sensor tip was aligned with the test seal surface, to prevent any influence on the flow, and to measure the temperature of the fluid in the lubrication film.

Because of the lack of texture on the non-textured seal, conditions related to temperature increase, such as film thickness and surface velocity, were expected to vary only in the radial direction. Therefore, measurement points on the non-textured seal were selected based only on the radial direction with no focus on the circumferential location of each point. The points, P_1, P_2, and P_3, were located at the same radial distances as the measurement points from the Rayleigh step and spiral groove test seals. The point, P_4, was located at the middle radius position of a dam on the Rayleigh step seal.

With the addition of texture, the film thickness and flow in the design of the Rayleigh step seal varied in the circumferential direction. Therefore, the measurement points were chosen based on the circumferential direction at different points related to the radial groove and the step. R_1 was located at the center of the radial groove, R_2 at the midpoint of the step, R_3 at the end of the step, and R_4 at the midpoint of the land. All points were set with the same radial distance from the midpoint of the step.

The measurement points on the spiral groove seal were chosen in the shape of spiral curve. The seal was designed to use texture to pump fluid from the inner to outer side of the seal; thus, measurement points were selected at various locations in the circumferential and radial directions. S_1 was located at the midpoint in both directions of the groove, and

S_2 was located at the midpoint of the land and the same radial distance of S_1. S_3 and S_4 were located at the intersections of the circle with the same radial distance as the midpoint of the dam and the extension of the spiral curve through S_1 and S_2, respectively.

Leakage rate was measured by collecting the fluid leaking into the inner side of the seal at 20 min from the start of the operation. During the operation, we confirmed that the temperature fluctuation was $\leq \pm 0.5$ °C for the last 30 s, the temperature increment reached a steady state. Turbine oil (ISO VG32) was used as the sealed fluid. The density of oil at 15 °C was 860.1 kg/m^3. Moreover, the kinematic viscosities of oil at 40 °C and 100 °C were 32.04 and 5.542 mm^2/s, respectively. Other experimental conditions are shown in Table 2.

2.4 Flow Visualization

To visualize the internal flow in the film, fluorescent particles (FA-203LF, SINLOIHI) were added to the sealed fluid as a tracer particle. The operation was started in the same manner as the temperature distribution measurement described in Sects. 2.2 and 2.3. Then, the lubrication film

Table 2 Experimental conditions

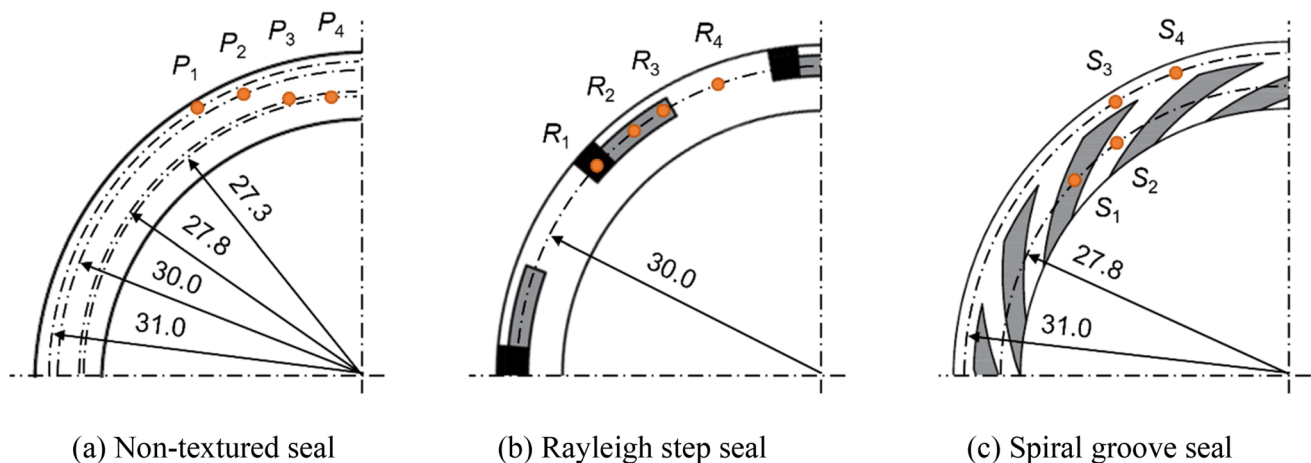|	
Rotational speed n_s	2000 and 2500/min
Surface velocity at outer radius u	6.7 and 8.3 m/s
Pressure in chamber p_o	20 kPa
Film thickness h_r	50 μm
Temperature of supplied oil T_{oil}	25 ± 2 °C
Temperature of atmospheric air T_{air}	23 ± 2 °C
Measuring time	20 min
Number of measurements	3

(a) Non-textured seal   (b) Rayleigh step seal   (c) Spiral groove seal

Fig. 4 Temperature measurement points

Table 3 Shooting conditions

Frame rate	10,000 fps
Shutter speed	50 μs
Spatial resolution	22 ± 1 μm/pixel

Table 4 Analytical conditions

Rotational speed n_s	2000 and 2500/min
Surface velocity at outer radius u	6.7 and 8.3 m/s
Outer pressure p_o	20 kPa
Inner pressure p_i	0 kPa
Oil density ρ	860.0 kg/m^3
Oil viscosity at 40 °C μ_a	27.5 mPa·s
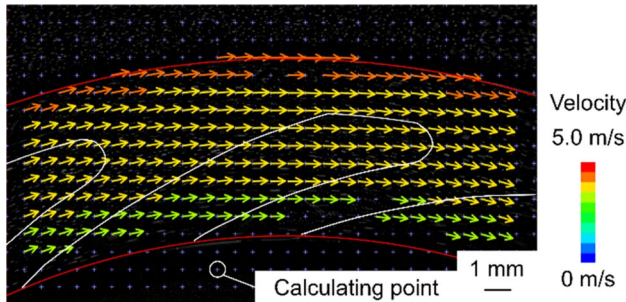
Fig. 5 Theoretical shear flow vectors

was irradiated with a 3.0 W sheet laser from the side of the equipment and shot by a high-speed camera (HX-6, nac Image Technology) from the top. The particle diameter was an average of 4 μm at a concentration of 0.025 g/L. Other shooting conditions are shown in Table 3. Fluorescent particles with an excitation wavelength of 530 nm were selected to match the laser wavelength of 532 nm. The longpass filter (O56, HOYA) was positioned between the film and camera lens. This filter, capable of filtering light of wavelengths < 560 nm (approximate), was also selected to match the fluorescence wavelength of 610 nm. Thus, it was possible to shoot particles while cutting out unnecessary reflected light.

In this study, the film thickness was 50 μm, which is larger than that in the mechanical seals used in practice, because tracer particles were used for flow visualization. However, because of the large outer diameter of the seal, the duty parameters in this study were approximately 3.3×10^{-5}–12×10^{-5}. Qiu et al. [4] tested the spiral grooved rings in the various duty parameters, 5.2×10^{-7}–4.2×10^{-4}, and showed that the rings could be operated in a fluid lubrication regime if the duty parameter was more than approximately 2.1×10^{-5}. Thus, the conditions adopted in our study is reasonable.

Particles in the captured images were used to calculate velocity vectors by PIV analysis (FlowExpert, KATOKO-KEN). The flow field on each test seal was evaluated by average velocity vectors for 10 rotations. The flow by pressure gradient was also estimated using the PIV analysis results. First, the velocity vectors of the shear flow due to rotation located at the midpoint of the film in the thickness direction were calculated at each calculating point as shown in Fig. 5. These vectors were obtained by halving the speed of
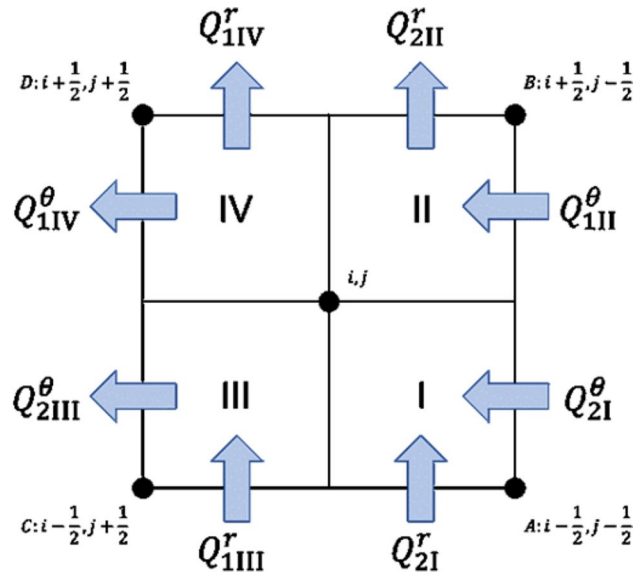

Fig. 6 Control volume and flow rates

a rotor surface. Next, the velocity components of the flow by pressure gradient were estimated by subtracting the theoretical velocity vector due to shear flow from the PIV analysis results. These vectors were used to evaluate variations in the flow field by processing the surface texture.

3 Numerical Analysis Method

In this study, the applicability of the isothermal numerical solutions was discussed. The solution was formulated through the divergence formulation method and adopted similarly as reported in a previous study [24]. The analysis conditions are shown in Table 4. The governing equation is the Reynolds equivalent equation for incompressible fluid and can be obtained using the equilibrium between the mass inflow and outflow rates of fluid entering and exiting the control volume due to the ring rotation:

$$Q_{2I}^r + Q_{1III}^r - Q_{2II}^r - Q_{1IV}^r + Q_{2I}^\theta + Q_{1II}^\theta - Q_{2III}^\theta - Q_{1IV}^\theta = 0 \tag{1}$$

Subscripts 1, 2 and I–IV in Eq. (1) indicate the domain in the control volume. The mass flow rates Q^r and Q^θ, shown in Fig. 6, can be obtained as follows:

$$Q^r = \int_{\theta_1}^{\theta_2} \rho \left(-\frac{h^3}{12\mu} \frac{\partial p}{\partial r} + \rho \frac{r\omega_s^2 h^3}{40\mu} \right) d\theta \qquad (2)$$

$$Q^\theta = \int_{r_1}^{r_2} \rho \left(-\frac{h^3}{12\mu r} \frac{\partial p}{\partial \theta} + \frac{r\omega_s h}{2} \right) dr \qquad (3)$$

Here, h is the total film thickness, which includes groove depth; r denotes the radius; ω_s denotes angular velocity; ρ denotes fluid density; and μ denotes fluid viscosity. Substituting Eqs. (2) and (3) into Eq. (1), the governing equation for pressure, p, is obtained. In the divergence formulation method, the mass flow rates of inflow and outflow corresponding to each domain are expressed by states at 4 midpoints, indicated as points A–D in Fig. 6. For example, Q^r_{2I} is discretized from Eq. (2) as follows:

$$Q^r_{2I} = \rho \left\{ -\frac{h_{i,j}^3}{12\mu} \frac{\partial p}{\partial r}\bigg|_A + \rho \frac{r_A \omega_s^2 h_{i,j}^3}{40\mu} \right\} \frac{\Delta \theta_{i,j-1}}{2} \qquad (4)$$

In Eq. (4), subscript A indicates the midpoint, $\Delta\theta$ denotes the lattice spacing in the circumferential direction. The state at each midpoint is expressed from 4 calculating points surrounding the midpoint, as follows:

$$r_A = \frac{r_{i,j} + r_{i-1,j} + r_{i,j-1} + r_{i-1,j-1}}{4}$$
$$\frac{\partial p}{\partial r}\bigg|_A = \frac{p_{i,j} - p_{i-1,j} + p_{i,j-1} - p_{i-1,j-1}}{2\Delta r_{i-1,j}} \qquad (5)$$

In Eq. (5), Δr denotes the lattice spacing in the radial direction. Other mass flow rates can be obtained similarly as Eqs. (4) and (5). Substituting the discretized mass flow rates into Eq. (1), the linear discretized equation for pressure, p, is obtained. The linear equation was solved by our Fortran program to obtain the pressure, p, at each calculating point.

Finally, the leakage rate q is obtained by the following integration:

$$q = \int_0^{2\pi} \left(-\frac{rh^3}{12\mu} \frac{\partial p}{\partial r}\bigg|_{r=r_i} + \rho \frac{r^2 \omega_s^2 h^3}{40\mu} \right) d\theta \qquad (6)$$

Similarly, as the mass flow rate of the film in the radial and circumferential directions can be obtained from the gradient of calculated pressure, p, the component of velocity due to the pressure gradient can be calculated by dividing mass flow rate by the density and cross-sectional area of the control volume. In addition, the component of
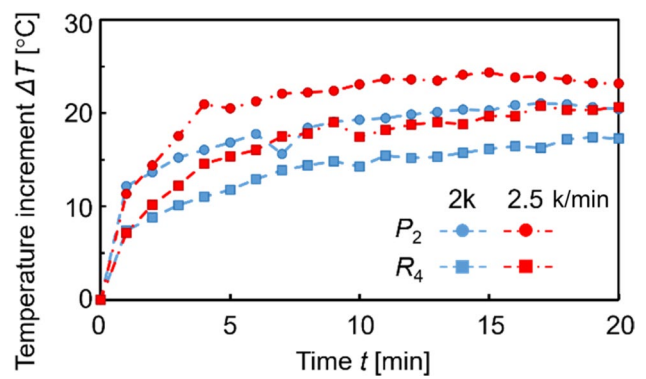

Fig. 7 Time variations of the temperature increments

Table 5 Thermal properties

Material	Stainless steel	Acrylic resin
Coefficient of thermal expansion α	$18.3 \times 10^{-7}/°C$	$70.0 \times 10^{-7}/°C$
Length of component L	12.0 mm	10.0 mm

velocity due to shear flow is obtained similarly as discussed in Sect. 2.4. Therefore, the velocity distribution in the film can be obtained by adding these components together.

However, in the experiment, the film thickness was expected to decrease because of thermal expansion, and the leakage rate was expected to decrease. Therefore, the film thickness and oil viscosity were adjusted on the basis of the temperature increments obtained in the experiment. Figure 7 shows the time variations of the temperature increments. The measurement points P_2 and R_4, which have the same radial distance and initial film thickness, were used as the reference for the temperature increments ΔT in each seal. The film thickness was set on the basis of the assumption that the test seal and rotor expand in accordance with temperature increment and that the film thickness decreases by the amount of length expansion ΔL, calculated from the following equation:

$$\Delta L = \alpha L \Delta T \qquad (7)$$

Here, α is the coefficient of thermal expansion and L is the length of each component. Table 5 shows the properties used for calculating the thermal expansion. The oil viscosity at each temperature is calculated from the reference viscosity μ_a and the following equation:

$$\mu = \mu_a e^{\gamma \Delta T} \qquad (8)$$

where γ is the temperature viscosity coefficient.

4 Results and Discussion

4.1 Comparison of Numerical and Experimental Leakage Rate

Figure 8 shows leakage rates with blue and red bars indicating results at 2000 and 2500/min, respectively. Bars indicate average values and error bars indicate maximum or minimum values on experimental results. Leakage rates for the spiral groove seal are not shown in the figure, because leakage to the inner side was not confirmed. Analytical values with thermal expansion of the non-textured seal are in good agreement with the experimental values quantitatively. However, both analytical values of the Rayleigh step seal did not agree quantitatively with the experimental results even though the decreasing trend of the leakage rate agreed with the increase in the rotational speed. Therefore, the numerical solution gave quantitatively consistent results for the non-textured seal considering the thermal expansion.

From the measured leakage rates, the Rayleigh step seal was confirmed to exhibit greater leakage rates than the non-textured seal. Furthermore, for increasing in rotational speeds, the leakage rate of the non-textured seal decreased, whereas that of the Rayleigh step seal increased. The leakage rate of the non-textured seal decreased with the increase in rotational speed, which may suggest that the flow of leakage to the inner side of the seal was inhibited by the increase in the centrifugal force acting on the sealed fluid. Conversely, the leakage rate increased for the Rayleigh step seal because its texture utilized hydrodynamic action, which increased with rotational speed.

4.2 Comparison with and Without Surface Texture

Figure 9 shows a comparison of temperature distributions with and without surface texture, indicating temperature
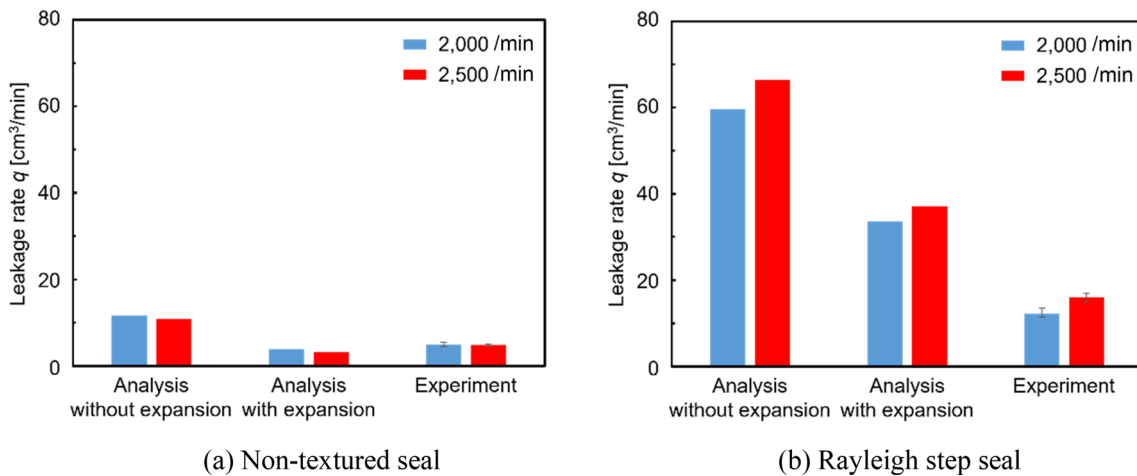

(a) Non-textured seal

(b) Rayleigh step seal

Fig. 8 Leakage rates

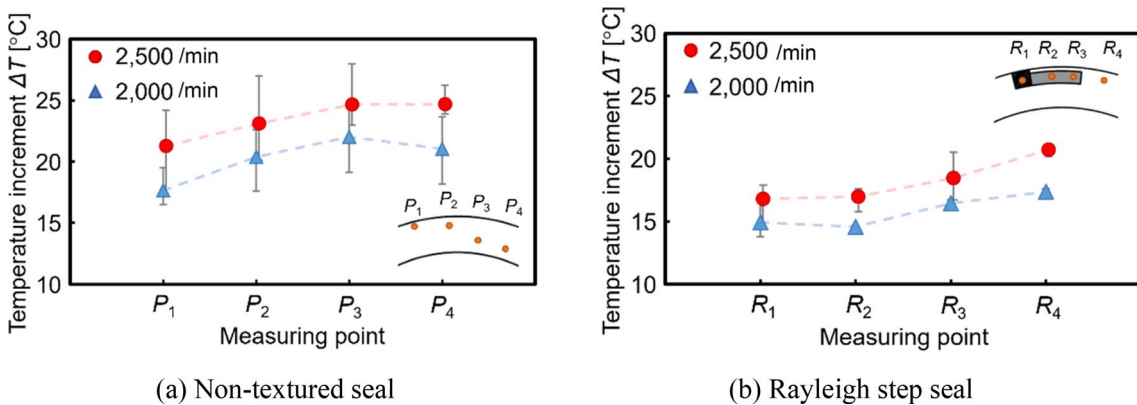(a) Non-textured seal

(b) Rayleigh step seal

Fig. 9 Comparison of temperature distribution with and without surface textures

increments after 20 min of operation at each measurement point. Figure 9a indicates that the temperature increment in the non-textured seal increased with proximity to the inner radius or at higher rotational speeds. The same tendency was observed in previous research on non-textured seals that were pressurized from the outer side because the outer side was cooled by sealed fluid [12]. In addition, the order of temperature increment, such as $P_4 > P_3 > P_2 > P_1$ at 2500/min, was the same in all three measurements for both rotational speeds in the non-textured seal. Therefore, the trend of temperature increments did not change in the circumferential direction, and the temperature distribution obtained with an axisymmetric lubrication film was also axisymmetric with no temperature differences in the circumferential direction. In contrast, the Rayleigh step seal in Fig. 9b shows different temperature increments in the circumferential direction, which corresponds to the design. Furthermore, all the temperature increments measured for the Rayleigh step seal were smaller than those corresponding to the same radial position for the non-textured seal, P_2, in Fig. 9a. However, the R_1 corresponding to the subsequent Rayleigh step, downstream of R_4, showed smaller temperature increment than that at the R_4. This indicated alternating low and high temperature areas in the entire ring-shape lubrication film. These results indicate that the difference in the flow field caused by surface textures affects the temperature distribution.

Flow visualization results are shown in Fig. 10. Red and white lines indicate the sealing face and textures,

respectively. The particles in the fluid lubrication film are shot with sufficient density for PIV analysis of each test seal; Fig. 11 shows the PIV analysis results. These vectors indicate flow direction and velocity, with the warmer vector colors indicating, higher velocities. Analytical results at 2500/min are shown in Fig. 12. Figure 12a and b indicate pressure distributions on each test seal, and Fig. 12c and d indicate flow fields obtained from the pressure distributions and shear speed. The analytical results were considering the thermal expansion and under the conditions for the last 1 min of the experiments. For the non-textured seal, the fluid flowed mostly in the circumferential direction. The flow in the radial direction induced by the pressure difference was small in comparison. Considering the greater temperature increments along with the flow in the Rayleigh step seal, the greater temperature increments in the non-textured seal is thought to be caused by not only heat transfer between the components with higher temperature on the inside and lower temperature on the outside but also gradual leaking of the fluid during heating as the fluid circled through the ring-shaped film as shown in Fig. 13a. Additionally, the velocity was slower and less heat was generated from shear stress on the inner side. Hence, the temperature increment was more strongly influenced by the time of heating, which is the elapsed time after the fluid flows into the lubrication film, than by the amount of heat generated by the shear stress at each point.
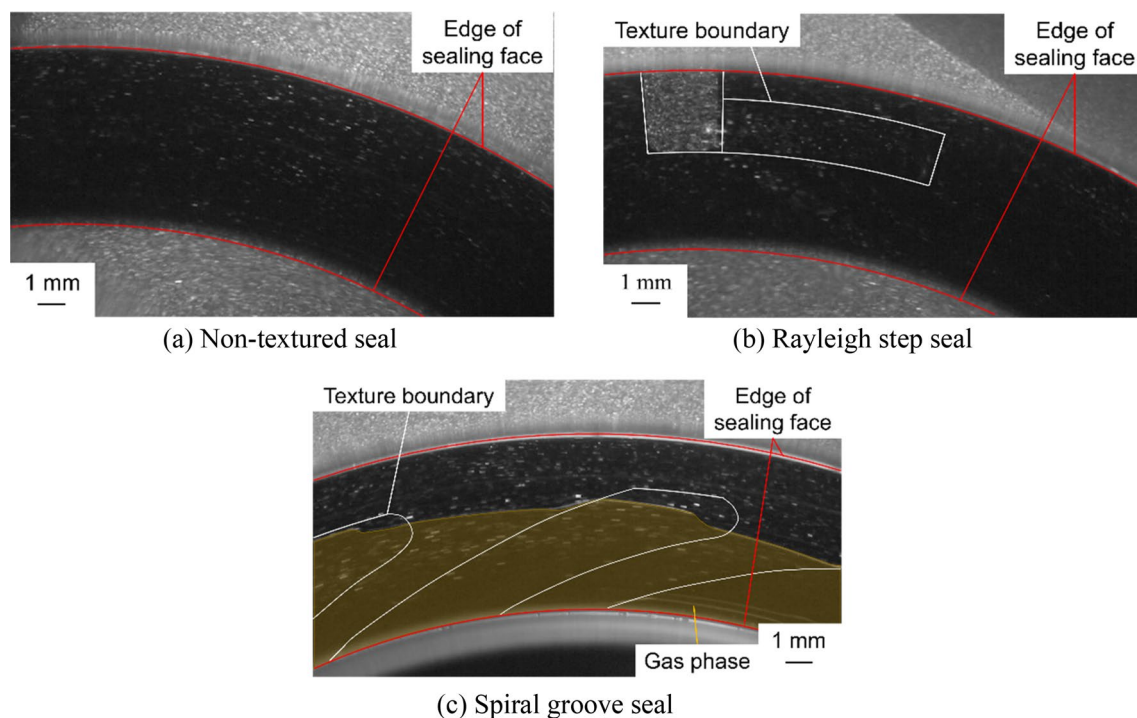

(a) Non-textured seal

(b) Rayleigh step seal

(c) Spiral groove seal

Fig. 10 Flow visualization results at 2,000/min

(a) Non-textured seal at 2,000 /min

(b) Non-textured seal at 2,500 /min

(c) Rayleigh step seal at 2,000 /min

(d) Rayleigh step seal at 2,500 /min
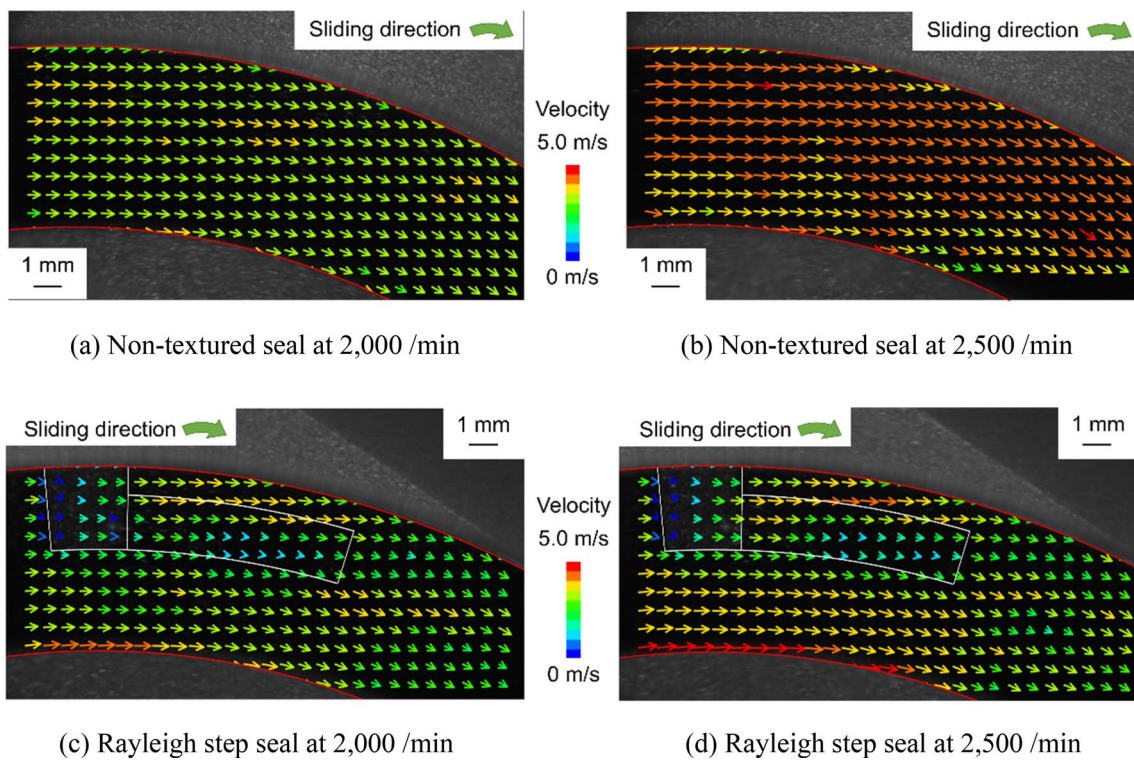
Fig. 11 Comparison of flow field with and without surface textures

(a) Pressure distribution of non-textured seal

(b) Pressure distribution of Rayleigh step seal

(c) Flow field of non-textured seal

(d) Flow field of Rayleigh step seal
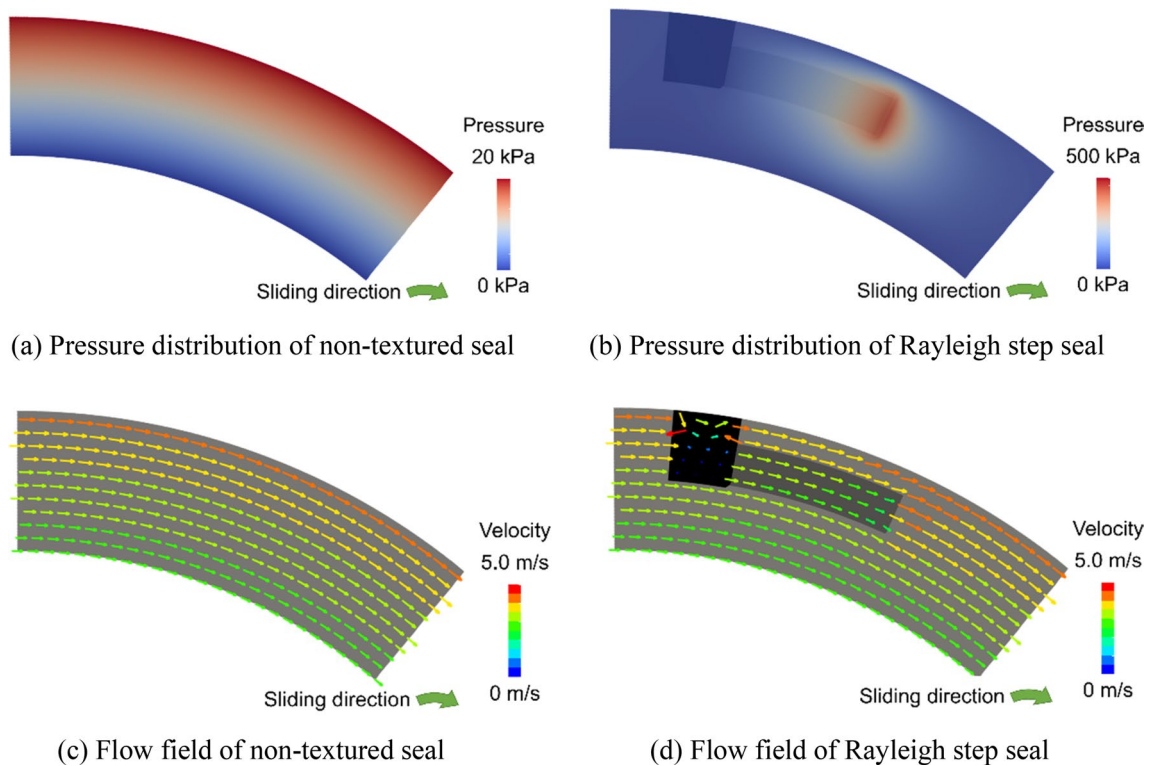
Fig. 12 Analytical results at 2,500/min

Fig. 13 Effect of internal flow in the lubrication film on temperature distribution

(a) Non-textured seal   (b) Rayleigh step seal
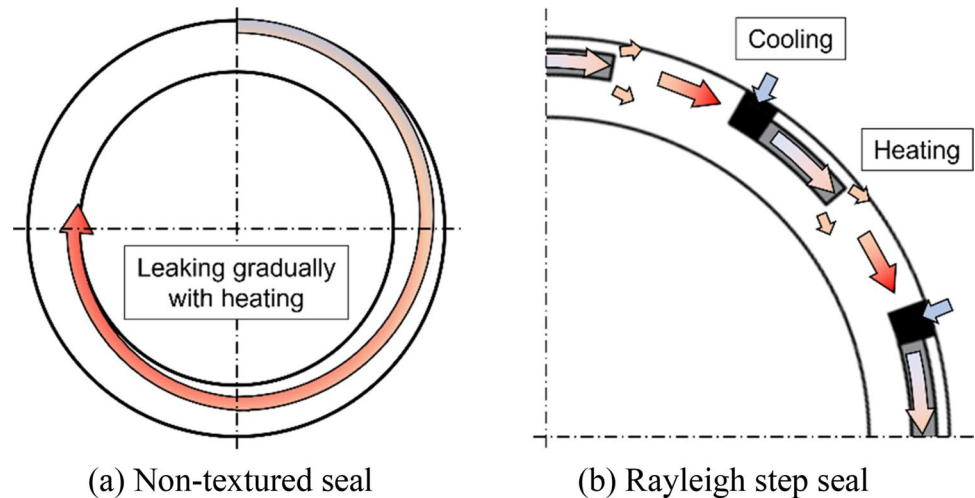
Meanwhile, for the Rayleigh step seal, the fluid was pumped into the radial groove caused by a vortex as shown in Fig. 14. This vortex was observed only in the experiments and was not observed in the analytical results, as shown in Fig. 12d, which uses the Reynolds equivalent equation and assumes a constant pressure in the film thickness direction. This pumping effect induced small temperature increments compared to the non-textured seal. Conversely, velocity vectors near the step moved toward the inner and outer sides, especially where the fluid was pumped out toward the outer side. The flow was considered to be caused by pressure increasing at the step located at the outside of the seal. Thus, the fluid flowed to a land or sealing dam through the radial groove and step as shown in Fig. 13b, explaining the larger temperature increment from R_1 to R_4. The temperature increase in the lubrication film can be suppressed by the effect of surface textures related to features such as the pumping effect. However, if the Rayleigh step seal is not improved to eliminate the deviation of the temperature distribution (as in the case of harsher conditions), there is also the risk of seal performance degradation or damage by contact because of thermal deformation and stress, similar to that reported in Ref. [8].

Here, the experimental and analytical results were similar with respect to the same flow direction at each area and

leakage rate, and showed a significant qualitative agreement. In addition, some of the results of the non-textured seal were also in quantitative agreement. However, in the Rayleigh step seal, the flow velocities did not agree quantitatively. In the analytical result, the velocities on the outer side were slower, for example, those near the end of the step were approximately 3.5 m/s whereas those in the experimental result were approximately 1.0 m/s. The pressure increase in the step might be underestimated in the analysis. Conversely, under the conditions of the Rayleigh step seal in a previous study [1], the solution with experimental results exhibited an error of approximately 2.5% and the numerical results agreed significantly with the experimental results. Differences between the two studies include large surface velocities and large thermal expansion coefficients of the material in the present study. Therefore, the present numerical solution might show quantitative deviations under conditions where complex flows occur, such as vortices in the radial groove as shown in Fig. 14, or thermal effects are significant. Not only simple film thickness estimation in the present study, but also high accuracy boundary conditions at the radial groove and estimation of the lubrication film shape during operation are necessary for quantitative agreement. The estimation of three-dimensional deformation is performed
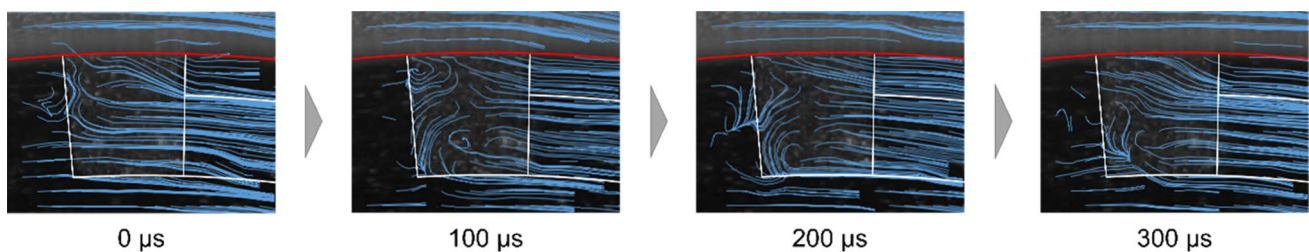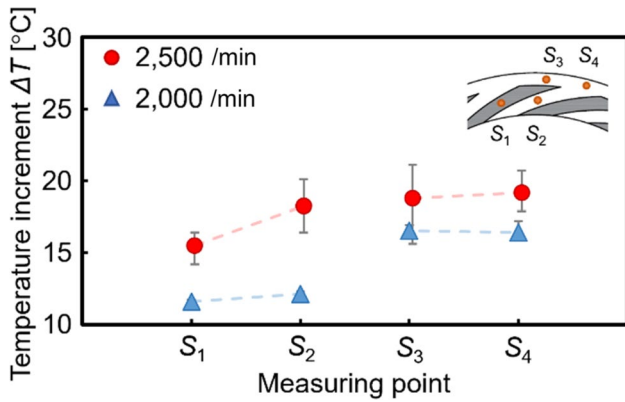

0 μs   100 μs   200 μs   300 μs

Fig. 14 Streamline in the radial groove

Fig. 15 Temperature distribution of spiral groove seal

Fig. 17 Flow field by pressure gradient at 2500/min

by coupling the energy equation and heat conduction equation.

4.3 Influence of Texture Geometry and Gas Phase

Figure 15 shows the temperature distribution of the spiral groove seal. When the rotational speed is 2000/min, the temperature increments at the two inner-side measurement points are smaller than those in all other test seals. By contrast, at a rotational speed of 2500/min, average temperature increments at S_2, S_3, and S_4 are ± 0.5 °C, which is equivalent to the accuracy of the thermocouple used in the experiments. This is the most homogeneous distribution confirmed in this study.

Figure 16 shows PIV analysis results for the spiral groove seal. Yellow areas indicate a gas phase of pumped atmospheric air. Figure 16a indicates the flow-field and gas-phase areas under 2000/min. Measurement point S_1 and S_2 are covered with atmospheric air. Hence, the lower temperature measurement results at these points indicate the temperature of the air, which has a lower dynamic viscosity than that of oil. Therefore, air pumped into the film led to an increase in the temperature difference. Similarly, at 2500/min shown in
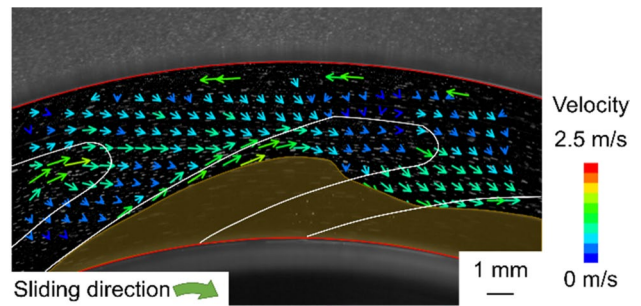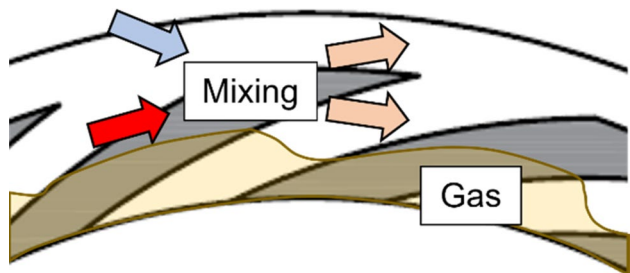

Fig. 18 Influence of texture geometry and gas phase

Fig. 16b, the air was pumped into the middle of the spiral grooves. Measurement point S_1, which exhibits smaller temperature increments than those at other measurement points, indicated the temperature of the air as well. These results indicate that the coexistence of gas and liquid phases in the lubrication film led to an increase in the temperature difference that was caused by the difference in dynamic viscosity.

Figure 17 shows the estimated flow field by pressure gradient for spiral groove seal under 2500/min. The flow field was calculated using the method described in Sect. 2.4 subtracting shear flow. The figure indicates that, except for the areas around the groove tip, the oil at the sealing dam flowed to the edge of the spiral grooves. The vectors around the groove tip oriented to avoid the tip through an increase
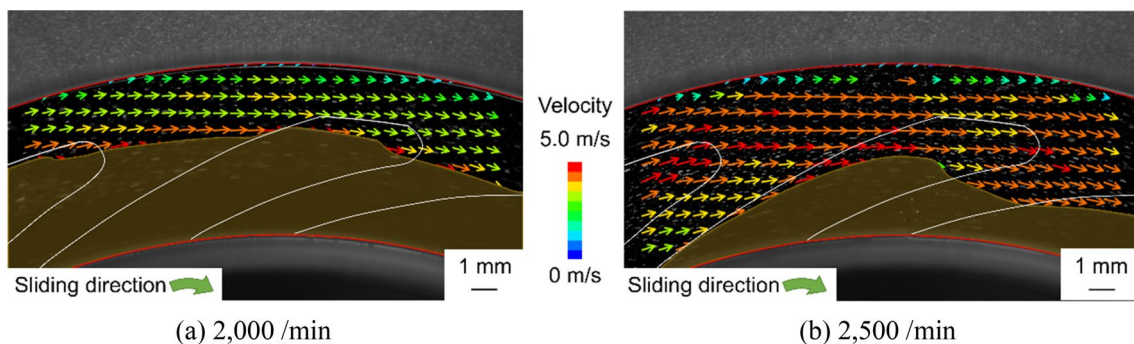

(a) 2,000 /min   (b) 2,500 /min

Fig. 16 PIV analysis results of spiral seal

Springer

in pressure, whereas, at the groove and land, the oil flowed to the edge of the groove in a similar fashion. However, note how the oil flows along the groove boundary and the oil–air interface. Overall, the oil flowed from the inner and outer sides toward the edge of the groove where it mixed, as shown in Fig. 18. Similar to the Rayleigh step, it then spread in the radial direction as the pressure increased. However, unlike the Rayleigh step seal, rising and falling pressure points were located at the center of the sealing face width, at narrow intervals. Therefore, the temperature distribution was relatively uniform because of the mixing of the warm fluid in the inner side and the cold fluid in the outer side. Thus, it can be observed that a uniform temperature distribution is more easily achieved when the fluid mixes before a large temperature difference is formed.

5 Conclusions

In this study, we observed the impacts of the flow field of a lubrication film on thermal variation, and compared the experimental results with numerical analysis results considering and not considering thermal expansion. Three types of surface patterns were evaluated from measurements of the temperature distribution and flow visualization, verifying the temperature distribution and flow field of each surface pattern. The following conclusions are drawn based on the findings of this study.

- For the non-textured seal, the fluid was observed to be circulating in the lubrication film and leaking into the inner side of the seal. In addition, larger temperature increments than that in the outer side were confirmed for areas in the vicinity of the inner side. The increments were 19% larger at the maximum compared to the outer side. Therefore, the elapsed time exerted a greater effect on the temperature increments of the film than the shear stress at each point and a tendency toward large temperature increments was observed in the downstream flow.
- For the Rayleigh step seal, the outer cooler fluid was pumped into the lubrication film at each radial groove, which decreased the film temperature. Therefore, the average temperature increment was approximately 26% lower than that of the non-textured seal. However, a temperature fluctuation of 23% was observed in the circumferential direction, caused by the cooling. Thus, the seal ring damage by thermal stress ought to be considered.
- The isothermal numerical solution including thermal expansion from the experimental data presented in this study was in good agreement with the experimental results in terms of leakage rate in the non-textured seal, and Raleigh step seal under the conditions such as slower surface velocities of the previous study [1]. However,

non-negligible quantitative deviations were observed in the Rayleigh step seal. This suggested that the importance of the complex flow including the effect of the outer boundary with thermal fluid effects in the numerical calculation in the case of textured seals. In other words, the present solution showed reasonable results under conditions without significant thermal effects or complex flow.

- The atmospheric air was pumped into the lubrication film and the gas phase was observed in the spiral groove seal. The observed temperature increments of the gas phase were 30% smaller than those of oil at the maximum. Therefore, the difficulty of temperature control of the seals increases, when there are two or more types of fluid with different properties in the lubrication film, such as oil and air.
- The spiral groove seal exhibited points where the pressure increased at the center of the sealing face width, at narrow intervals. Thus, the fluid spread frequently in the radial direction, resulting in the mixing of the outer cold fluid with the inner warm fluid. Therefore, the temperature differences in the oil at each measurement point in the spiral groove seal was within ± 0.5 °C, which was the most homogeneous temperature distribution in this study.

In this way, the temperature distribution of a flow field in a lubrication film can be controlled by the surface texture shape or depth. The reliability of lubrication films exposed to thermal variations can be improved through the design of textures that achieve higher performance. In this study, above mentioned findings were obtained by the experiments. Nevertheless, evaluation and findings under the environment similar to real seals leading to textures with higher reliability will be possible in the future by utilizing the photochromic visualization technique [25, 26], which uses a dye that does not affect the flow, and by selecting suitable materials and devices for the technique. Meanwhile, it is also important to improve the applicability of the numerical solution toward other operating conditions and sealed fluid. Specifically, the energy equation, the heat conduction equation of the seal ring, and appropriate outer environmental effects should be introduced. In addition, the analytical solution should be improved to accommodate gas–liquid two-phase flow, as observed in the spiral groove seal, to enable high accuracy comparisons with experiments and to identify textures with high reliability.

Declarations

Conflict of Interest The authors have no relevant financial or non-financial interests to disclose.

References

1. Ikeuchi, K., Mori, H., Nishida, T.: A Rayleigh-step face seal with reverse steps. JSME Int. J. (1987). https://doi.org/10.1299/jsme1987.30.2027

2. Buck, G.S., Volden, D.: Upstream pumping: a new concept in mechanical sealing technology. Lubr. Eng. **46**(4), 213–217 (1990)

3. Tokunaga, Y., Inoue, H., Okada, K. Uemura, N., Yamamoto, Y.: Improvement in sealing performance and friction reduction by laser surface texturing for mechanical seal. Proc. 21st Int. Conf. Fluid Seal. 91–102 (2011)

4. Qiu, Y., Khonsari, M.M.: Investigation of tribological behaviors of annular rings with spiral groove. Tribol. Int. (2011). https://doi.org/10.1016/j.triboint.2011.05.008

5. Lai, T.: Development of non-contacting, non-leaking spiral groove liquid face seals. Lubr. Eng. **50**(8), 625–631 (1994)

6. Meng, X., Bai, S., Peng, X.: Lubrication film flow control by oriented dimples for liquid lubricated mechanical seals. Tribol. Int. (2014). https://doi.org/10.1016/j.triboint.2014.04.020

7. Kanda, K., Tazawa, S., Urano, T., Kobayashi, S., Adachi, K.: The possibility of both low friction and low leakage by surface texture of mechanical seals in blood. Tribol. Lett. (2020). https://doi.org/10.1007/s11249-020-01289-7

8. Mayer, E.: Mechanical seals. Butterworth-Heinemann, Oxford (1977)

9. Zhang, G., Chen, G., Zhao, W., Yan, X., Zhang, Y.: An experimental test on a cryogenic high-speed hydrodynamic non-contact mechanical seal. Tribol. Lett. (2017). https://doi.org/10.1007/s11249-017-0865-1

10. Blasiak, S., Kudera, C.: A numerical analysis of the grooved surface effects on the thermal behavior of a non-contacting face seal. Procedia Eng. (2012). https://doi.org/10.1016/j.proeng.2012.07.037

11. Zhou, J., Gu, B., Chen, Y.: An improved design of spiral groove mechanical seal. Chin. J. of Chem. Eng. (2007). https://doi.org/10.1016/S1004-9541(07)60115-3

12. Adjemout, M., Brunetiêre, N., Bouyer, J.: Friction and temperature reduction in a mechanical face seal by a surface texturing: comparison between TEHD simulations and experiments. Tribol. Trans. (2018). https://doi.org/10.1080/10402004.2018.1478053

13. Teshima, Y.: The research on sealing characteristics with dimple sliding materials in mechanical seals. Nagasaki University (2000). (**in Japanese**)

14. Christensen, H.: Stochastic models for hydrodynamic lubrication of rough surfaces. Proc. Inst. Mech. Eng. (1969). (**in Japanese**) https://doi.org/10.1243/PIME_PROC_1969_184_074_02

15. Patir, N., Cheng, H.S.: An average flow model for determining effects of three-dimensional roughness on partial hydrodynamic lubrication. J. Lubr. Tech. (1978). https://doi.org/10.1115/1.3453103

16. Tokunaga, Y., Inoue, H., Okada, K., Shimomura, T., Yamamoto, Y.: Effects of cavitation ring formed on laser-textured surface of mechanical seal. Tribol. Online. (2011). https://doi.org/10.2474/trol.6.36

17. Cross, A.T., Sadeghi, F., Cao, L., Rateick, R.G., Jr., Rowan, S.: Flow visualization in a pocketed thrust washer. Tribol. Trans. (2012). https://doi.org/10.1080/10402004.2012.681343

18. Richardson, D., Sadeghi, F., Rateick, R.G., Jr., Rowan, S.: Using μPIV to investigate fluid flow in a pocketed thrust bearing. Tribol. Trans. (2019). https://doi.org/10.1080/10402004.2018.1556370

19. Ochiai, M., Namai, T., Hashimoto, H.: Visualization experiment of gas flow on dry gas seal under sinusoidal excitation conditions. Tribologist. (2019). https://doi.org/10.18914/tribologist.19-00006

20. Strubel, V., Simoens, S., Vergne, P., Fillot, N., Ville, F., El Hajem, M., Devaux, N., Mondelin, A., Maheo, Y.: Fluorescence tracking and μ-PIV of individual particles and lubricant flow in and around lubricated point contacts. Tribol. Lett. (2017). https://doi.org/10.1007/s11249-017-0859-z

21. Walowit, J.A., Pinkus, O.: Analysis of face seals with shrouded pockets. J. Lubr. Tech. (1982). https://doi.org/10.1115/1.3253190

22. Strom, T.N., Ludwig, L.P., Johnson, R.L.: Spiral groove face seal concepts; comparison to conventional face contact seals in sealing liquid sodium (400 to 1000 Deg F). J. Lubr. Tech. (1968). https://doi.org/10.1115/1.3601580

23. Salant, R.F., Homiller, S.J.: Stiffness and leakage in spiral groove upstream pumping mechanical seals. Tribol. Trans. (1993). https://doi.org/10.1080/10402009308983132

24. Hashimoto, H., Ochiai, M.: Optimization of groove geometry for thrust air bearing to maximize bearing stiffness. J. of Tribol. (2008). https://doi.org/10.1115/1.2913546

25. Azetsu, A., Kitajima, I., Kuratsuji, K.: Development of a new visualization technique using photochromism for transport process of lubricating oil around the engine piston. Int. J. Engine Res. (2019). https://doi.org/10.1177/1468087418819229

26. Muraoka, N., Ochiai, M.: Effect of oil film behavior on roller surface on cooling in traction drives. J. Adv. Mech. Des. Syst. Manuf. (2020). https://doi.org/10.1299/jamdsm.2020jamdsm0038